European Journal of Mechanics A/Solids 39 (2013) 218–228

Contents lists available at SciVerse ScienceDirect

European Journal of Mechanics A/Solids

journal homepage: www.elsevier.com/locate/ejmsol

Structural analysis using a dipolar elastic Timoshenko beam

A. Triantafyllou [a,b], A.E. Giannakopoulos [b,*]

[a] Department of Civil Engineering, Laboratory of Reinforced Concrete Technology and Structures, University of Thessaly, Volos 38336, Greece
[b] Department of Civil Engineering, Laboratory for Strength of Materials and Micromechanics, University of Thessaly, Volos 38336, Greece

ARTICLE INFO

Article history:
Received 28 May 2012
Accepted 28 November 2012
Available online 12 December 2012

Keywords:
Dipolar strain gradient elasticity
Timoshenko beam
Microcantilevers

ABSTRACT

In recent years, several non-local beam theories have emerged in trying to model stiffness and strength phenomena observed in micro-beams used in micro-mechanical systems (MEMS) and sensors. Of particular importance are the theories that treat in a unified way both long and short beams, through Timoshenko beam kinematics. At the same time and in combination with experiments, beam models have been used to estimate material lengths that are necessary for the assessment of non-local elasticity theories. Aside from the particular details of the non-local assumptions used, boundary conditions play a considerable role in such problems, especially the non-classical boundary conditions that are required by the non-local theories. It is astonishing how few and simple beam configurations have been presented so far. They fall in the category of statically determinate beams and their key results are often given in the form of Fourier series, making it hard for the designers of MEMS to use these results and expand them into more complex beam systems like frames, grids, etc. It is the scope of this work to present closed-form solutions to the Timoshenko beam problem, based on dipolar strain gradient elasticity and show how to treat statically indeterminate problems in a consistent manner.

1. Introduction

The term “size effect” is used to describe the dependence of the mechanical behavior of a member to its microstructure. When the dimensions of the microstructure (grain size, inclusion size, lattice distance etc.) become comparable with the dimensions of the member itself, the assumption of a homogeneous medium of classical elasticity and its implication concerning the very definition of stress and strain no longer suffice. In other words as structures are scaled down, their behavior becomes increasingly dominated by the inhomogeneous nature of the material itself. The need to model such behavior without modeling the full detail of the microstructure has led to the development of enriched continuum models. This is done in an average sense by introducing length scale parameters in the constitutive equations that account for the effect that the microstructure has on the deformation process. By doing so, these theories have the advantage over classical elasticity of explaining why smaller structures are stiffer. However, in their original form (Mindlin, 1964; Cosserat and Cosserat, 1909; Eringen, 1966; Koiter, 1964) these theories become unpractical since it is impossible to quantify all these new length scale parameters with the available experimental practices, i.e. static or dynamic bending tests. Nevertheless, by simplifying these theories to a minimum, e.g. keeping just one length scale parameter (for static cases), calibration becomes possible and at the same time the key novelty of such theories which is the prediction of size effect is preserved. For this reason, in this work, we use a simplified (dipolar) isotropic strain gradient theory with just one material length scale parameter g, in addition to the two classical elasticity parameters (the elastic modulus E and the Poisson's ratio ν).

Small structural elements that are used in the design of micro electromechanical systems (MEMS) are often in the form of beams (e.g. sensors and actuators) and their design requires them to deform within their elastic domain (Senturia, 2001). Although the stiffness of such micro devices is essential information for their design, in many cases their stiffness was determined experimentally and was found to be higher than that predicted by classical elasticity. Salvetat et al. (1999) performed bending experiments on single walled carbon nanotube beams with both ends fixed arranged in a close-packed lattice (dimensions of the lattice unit was 1.4 nm) and used different rope diameters, from 3 to 20 nm, in bending experiments. They found that as the diameter decreased the nanotubes exhibit a much stiffer response. The same behavior was observed in carbon nanotubes by Poncharal et al. (1999). Ding et al. (2001a) tested polysilicon microcantilevers (grain size of polysilicon is in the order of 0.2 μm) with thickness of 2.4 μm and variable aspect ratios and although the authors attributed the stiffness differences between the beams to measurement errors, a closer look at their results suggests the existence of size effect.

* Corresponding author. Tel.: +30 24210 74179; fax: +30 24210 74169.
E-mail address: agiannak@uth.gr (A.E. Giannakopoulos).

0997-7538/$ – see front matter © 2012 Elsevier Masson SAS. All rights reserved.
http://dx.doi.org/10.1016/j.euromechsol.2012.11.011

Lam et al. (2003) performed bending tests on epoxy polymeric microcantilevers with thickness varying from 20 to 115 μm and showed that as the thickness of the beam decreased the stiffness increased beyond the predictions of classical elasticity. Although no information about the microstructure of the PP microcantilevers is included in this work, high crosslink-density regions from 6 to 104 nm in diameter have been observed in cross-linked resins forming a heterogeneous rather than a homogeneous material on that scale (Morgan and O'Neal, 1977; Vanlandingham et al., 1999). McFarland and Colton (2005) tested polypropylene (PP) microcantilevers which have a non-homogeneous microstructure due to their semi-crystalline nature and found that the microcantilevers with thickness of 15 and 29 μm exhibit a much stiffer response which can not be explained by any of the possible error sources associated with the experiments. It is noted that the non-homogeneous nature of PP is due to the formation of spherical particles called spherulites during its manufacturing process. The authors did not provide any information about the size of the spherulites in their material but typically their size can be up to 10 μm when manufacturing of the specimen is via injection molding (Vianna et al., 2002). Hong et al. (2005) tested copper (Cu) microcantilevers with thickness of 10.5 and 2.8 μm in bending and reported on the thinner films having a stiffer response. Grain size of copper films manufactured by electroplating and annealed in vacuum can be up to 1 μm (Perez-Prado and Vlassak, 2002). Yang et al. (2008) tested native and cross-linked type I collagen fibrils with diameters ranging from 187 to 424 nm and found that the stiffness increased as the diameter of the fibrils decreased. Note that collagen fibrils are assembled of parallel collagen molecules arranged with a longitudinal stagger and also contain mineral particles (typically flat and elongated) with the elongated dimension reaching values up to 100 nm (Jager and Fratzl, 2000). It is also worth mentioning the work of Namarazu et al. (2000) and Liu et al. (2008) who carried out bending experiments on single crystal silicon beams which have a continuous crystal lattice (no grain boundaries) and hence can be seen as completely homogeneous and found absence of size effect in stiffness as the specimens ranged from a nano- to a milli-meter scale (size effect on the strength on the other hand was significant). This review of the available experimental evidence is not meant to be exhaustive but only indicative of the phenomenon which the current work attempts to explain, which is that size effect in the elastic deformation range of beams is to be expected when the scale of the structure becomes comparable with the scale of the microstructure.

The need to quantify the departure from the classical elasticity predictions and offer the designer of MEMS a theoretical tool in the form of close form solutions for predicting size effect is the main motivation for this work. We are interested in the solution of a Timoshenko beam (Timoshenko and Goodier, 1970) loaded statically. Papargyri-Beskou et al. (2003) have used the same simplified strain gradient theory with surface energy (Vardoulakis and Sulem, 1995) to solve the bending and buckling of the Bernoulli–Euler beam. Their model has been investigated further by Giannakopoulos and Stamoulis (2006) for the case of cantilever beam bending and stretching of a cracked bar. Nevertheless, the Bernoulli–Euler beam is only applicable to slender beams where shear forces have a negligible influence on the deformation of the beam. The present work with the use of the Timoshenko beam kinematics examines how the gradient solution is affected when the shear forces are included in the analysis. It is noted here that the same strain gradient elasticity theory has been used by Wang et al. (2010) and Lazopoulos and Lazopoulos (2011) for the case of Timoshenko beam kinematics. Both these works employ Fourier series to solve the boundary value problem whereas in the present work closed-form solutions are provided. Furthermore, none of these works address the issue of hyperstatic members and how they should be treated and only refer to the isostatic case of a simple supported beam. As it would become apparent, by solving the problem in a closed-form, a methodology for treating more complex structural problems (hyperstatic beams, frames etc.) emerges. However, it is beyond the scope of this work to explore all beam configurations and only the example of a doubly-clamped beam is considered in detail. Other differences concerning the solution between the present theory and the two works mentioned above also exist and are discussed in detail in Section 4. Finally, other non-local theories for the case of Timoshenko beam kinematics have also been considered by Lam et al. (2003), Reddy (2007), Ma et al. (2008), Asghari et al. (2011), Ramezani et al. (2009). These works employ different gradient elasticity theories than the present and are briefly discussed in Section 4. Models that are based on integral (strong) non-local theories will not be examined in this work.

This paper is structured as follows: In Section 2, we derive the governing equations and boundary conditions for the Timoshenko beam. In Section 3, we apply our model to the specific problem of a cantilever beam with a point load at its free end and investigate the details of the solution. We also investigate a hyperstatic beam, i.e. a beam clamped at both ends, loaded by a point load in the middle. In Section 4, we compare the present approach with the various Timoshenko beam theories that exist in the literature. Finally, in Section 5, we use experimental data on microcantilevers available in the literature in order to compare the predictions of the length parameter of the strain gradient elasticity with the corresponding predictions of the micropolar elasticity.

2. Governing equations and boundary conditions

We consider a straight prismatic beam subject to a static lateral load $q(x)$ distributed along the longitudinal axis x of the beam, as shown in Fig. 1(a). The loading plane coincides with the xz plane and the cross section of the beam is parallel to the yz plane. Both the geometry and the loading of the beam are symmetric with respect to the plane xz. The displacement field following the Timoshenko beam kinematics can be described by the following relations:

$$\begin{aligned} u_x &= z\psi(x) \\ u_y &= 0 \\ u_z &= w(x) \end{aligned} \tag{1}$$

where $\psi(x)$ is the rotation angle of the cross section with respect to the vertical z-direction and $w(x)$ is the z component of the displacements. Note that the Timoshenko kinematics prevent the appearance of boundary conditions at the prismatic surface of the beam and so boundary conditions become relevant only on the beam's cross section at the two ends, keeping the one-dimensional character of the solution. It is beyond the scope of this work to solve analytically the true three-dimensional (3D) problem. The important question is whether such approach is justified and this question is addressed by comparing the predictions of the present model with the 2D finite element results, which suffice for the case of beams (see Fig. 8).

Using the geometric relations (Eq. (1)), the non-zero axial and shear strains are equal to:

$$\begin{aligned} \varepsilon_{xx} &= \frac{\partial u_x}{\partial x} = z\frac{d\psi}{dx} \\ \gamma_{xz} &= 2\varepsilon_{xz} = \frac{\partial u_x}{\partial z} + \frac{\partial u_z}{\partial x} = \frac{dw}{dx} + \psi \end{aligned} \tag{2}$$

The material is a homogeneous, linear elastic material and the non-zero Cauchy stresses are equal to:

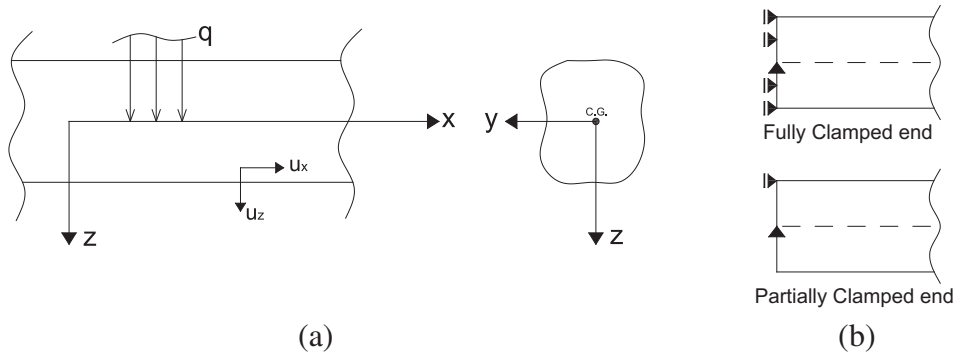

Fig. 1. (a) Beam configuration and coordinate system. (C.G.: center of gravity), (b) Possible clamped configurations.

$$\overline{\sigma}_{xx} = E\varepsilon_{xx} \tag{3a}$$

$$\overline{\sigma}_{xz} = kG\gamma_{xz} \tag{3b}$$

where k is a correction factor which depends on the shape of the beam section and the Poisson's ratio ν (Kaneko, 1975) introduced to account for the non-uniformity of the shear strain over the beam's cross section, E is the Young's modulus of elasticity and G the shear modulus. It is recalled that for an isotropic material $G = E/2(1+\nu)$. Note that Eq. (3a) is based on the assumption of Poisson's ratio being zero. Eq. (3a) can be modified to account for the effect of isotropic Poisson's ratio (as in Ma et al., 2008), if $E^* = ((1-\nu)/(1+\nu)(1-2\nu))E$ is used instead of E. We will keep the simplified form of Eq. (3a) but throughout the manuscript the numerical results are derived using E^*.

The employed strain gradient theory is a simplification of Mindlin's (1964) form II gradient theory, using just one material length scale parameter. In this case, the non-zero total axial and shear stresses can be casted, with respect to the Cauchy stresses (see related discussion in Ru and Aifantis, 1993; Papargyri-Beskou et al., 2009), as:

$$\begin{aligned} \sigma_{xx} &= (1-g^2\nabla^2)\overline{\sigma}_{xx} \\ \sigma_{xz} &= (1-g^2\nabla^2)\overline{\sigma}_{xz} \end{aligned} \tag{4}$$

where g is the strain gradient material length, the over bar quantities are the Cauchy stresses (see Eqs. (3a–b)) and $\nabla^2 = \partial^2/\partial x^2 + \partial^2/\partial z^2$ is the Laplace operator.

The total internal elastic strain energy of the beam is:

$$U_{\text{tot}} = U_{\text{cl}} + U_{\text{gr}} \tag{5}$$

where U_{cl} is the internal elastic strain energy of a classical beam and is equal to:

$$U_{\text{cl}} = \frac{1}{2}\iiint_V (\overline{\sigma}_{xx}\varepsilon_{xx} + 2\overline{\sigma}_{xz}\varepsilon_{xz})\mathrm{d}x\mathrm{d}y\mathrm{d}z \tag{6}$$

and U_{gr} is the internal elastic strain energy of a purely gradient beam and is equal to:

$$U_{\text{gr}} = \frac{1}{2}g^2\iiint_V \left(\frac{\partial\overline{\sigma}_{xx}}{\partial x}\frac{\partial\varepsilon_{xx}}{\partial x} + 2\frac{\partial\overline{\sigma}_{xz}}{\partial x}\frac{\partial\varepsilon_{xz}}{\partial x} + \frac{\partial\overline{\sigma}_{xx}}{\partial z}\frac{\partial\varepsilon_{xx}}{\partial z}\right)\mathrm{d}x\mathrm{d}y\mathrm{d}z \tag{7}$$

The variation of the total elastic strain energy for a beam of length L is:

$$\begin{aligned} \delta U_{\text{tot}} = \int_0^L \Bigg\{ & \delta\psi\left(-EI\left(1-g^2\frac{\mathrm{d}^2}{\mathrm{d}x^2}\right)\frac{\mathrm{d}^2\psi}{\mathrm{d}x^2} + kAG\left(1-g^2\frac{\mathrm{d}^2}{\mathrm{d}x^2}\right)\left(\frac{\mathrm{d}w}{\mathrm{d}x}+\psi\right) - EAg^2\frac{\mathrm{d}^2\psi}{\mathrm{d}x^2}\right) + \delta w\left(-kAG\left(1-g^2\frac{\mathrm{d}^2}{\mathrm{d}x^2}\right)\left(\frac{\mathrm{d}^2w}{\mathrm{d}x^2}+\frac{\mathrm{d}\psi}{\mathrm{d}x}\right)\right)\Bigg\}\mathrm{d}x \\ & + \left[\delta\psi\left(EI\left(1-g^2\frac{\mathrm{d}^2}{\mathrm{d}x^2}\right)\frac{\mathrm{d}\psi}{\mathrm{d}x} + kAGg^2\left(\frac{\mathrm{d}^2w}{\mathrm{d}x^2}+\frac{\mathrm{d}\psi}{\mathrm{d}x}\right) + EAg^2\frac{\mathrm{d}\psi}{\mathrm{d}x}\right)\right]_0^L + \left[\delta w\left(kAG\left(1-g^2\frac{\mathrm{d}^2}{\mathrm{d}x^2}\right)\left(\frac{\mathrm{d}w}{\mathrm{d}x}+\psi\right)\right)\right]_0^L \\ & + \left[\delta\psi'\left(g^2EI\frac{\mathrm{d}^2\psi}{\mathrm{d}x^2}\right)\right]_0^L + \left[\delta w'\left(kAGg^2\left(\frac{\mathrm{d}^2w}{\mathrm{d}x^2}+\frac{\mathrm{d}\psi}{\mathrm{d}x}\right)\right)\right]_0^L \end{aligned} \tag{8}$$

where δ indicates variation, I is the second moment of inertia about the z-axis ($I = \iint z^2\mathrm{d}y\mathrm{d}z$) and A is the cross section area ($A = \iint \mathrm{d}y\mathrm{d}z$). Eq. (8) is obtained from Eq. (5), using Eqs. (6) and (7) by expressing all quantities through the independent kinematic variables w, ψ, w' and ψ' and applying integration by parts. Note that classic analysis uses only w and ψ as independent kinematic variables.

The variation of the work δW done by the distributed forces $q(x)$, by the classical and non-classical boundary shear forces Q and Y respectively and by the classical and non-classical bending moments M and m, respectively, is:

$$\delta W = \int_0^L q\delta w\mathrm{d}x + [Q\delta w]_0^L + [M\delta\psi]_0^L + [Y\delta w']_0^L + [m\delta\psi']_0^L \tag{9}$$

The principle of minimum potential energy states:

$$\delta(U_{\text{tot}} - W) = 0 \tag{10}$$

It is recalled that in classic elasticity, the bending moment $\overline{M}$ and shear forces $\overline{Q}$ are equal to:

$$\begin{aligned} \overline{M} &= \iint_A \overline{\sigma}_{xx} z \, \mathrm{d}A = EI\frac{\mathrm{d}\psi}{\mathrm{d}x} \\ \overline{Q} &= \iint_A \overline{\sigma}_{xz} \mathrm{d}A = kAG\left(\frac{\mathrm{d}w}{\mathrm{d}x} + \psi\right) \end{aligned} \tag{11}$$

Substituting Eqs. (8) and (9) into Eq. (10) and using Eq. (11), we derive the following governing equations (i.e. Eqs. (12a–b)) and boundary conditions (i.e. Eqs. (13a–d)) for the gradient Timoshenko beam:

$$\left(1 + \frac{A}{I}g^2 - g^2\frac{\mathrm{d}^2}{\mathrm{d}x^2}\right)\frac{\mathrm{d}\overline{M}}{\mathrm{d}x} = \left(1 - g^2\frac{\mathrm{d}^2}{\mathrm{d}x^2}\right)\overline{Q} \tag{12a}$$

$$\left(1 - g^2\frac{\mathrm{d}^2}{\mathrm{d}x^2}\right)\frac{\mathrm{d}\overline{Q}}{\mathrm{d}x} = -q \tag{12b}$$

$$\left[\left\{Q - \left(\left(1 - g^2\frac{\mathrm{d}^2}{\mathrm{d}x^2}\right)\overline{Q}\right)\right\}\delta w\right]_0^L = 0 \tag{13a}$$

$$\left[\left\{Y - \left(g^2\frac{\mathrm{d}\overline{Q}}{\mathrm{d}x}\right)\right\}\delta w'\right]_0^L = 0 \tag{13b}$$

$$\left[\left\{M - \left(\left(1 - g^2\frac{\mathrm{d}^2}{\mathrm{d}x^2}\right)\overline{M} + \frac{A}{I}g^2\overline{M} + g^2\frac{\mathrm{d}\overline{Q}}{\mathrm{d}x}\right)\right\}\delta\psi\right]_0^L = 0 \tag{13c}$$

$$\left[\left\{m - \left(g^2\frac{\mathrm{d}\overline{M}}{\mathrm{d}x}\right)\right\}\delta\psi'\right]_0^L = 0 \tag{13d}$$

Note that all the above relations reduce to the classic Timoshenko beam expressions in the absence of gradient, i.e. $g = 0$. Also note that the coefficient A/I scaling the g^2 in Eqs. (12a) and (13c) stems directly from the cross term $(\partial\overline{\sigma}_{xx}/\partial z)(\partial\varepsilon_{xx}/\partial z)$ in the expression of the strain gradient elastic energy (Eq. (7)). Considering only the leading gradient shear term, i.e. $(\partial\overline{\sigma}_{xz}/\partial x)(\partial\varepsilon_{xz}/\partial x)$, will not capture this additional scaling effect of the shear. Therefore, for a complete gradient Timoshenko beam solution both terms must be considered.

The boundary conditions (Eqs. (13a–d)) are mutually exclusive. This means that one can prescribe:

$$Q = \left(1 - g^2\frac{\mathrm{d}^2}{\mathrm{d}x^2}\right)\overline{Q} \text{ or } w \tag{14a}$$

$$Y = \left(g^2\frac{\mathrm{d}\overline{Q}}{\mathrm{d}x}\right) \text{ or } w' \tag{14b}$$

$$M = \left(1 - g^2\frac{\mathrm{d}^2}{\mathrm{d}x^2}\right)\overline{M} + \frac{A}{I}g^2\overline{M} + g^2\frac{\mathrm{d}\overline{Q}}{\mathrm{d}x} \text{ or } \psi \tag{14c}$$

$$m = g^2\frac{\mathrm{d}\overline{M}}{\mathrm{d}x} \text{ or } \psi' \tag{14d}$$

Table 1, summarizes the end conditions and continuity requirements that stem from the boundary conditions (Eqs. 14a–d) for a gradient Timoshenko beam. This table is of utmost importance for solving beam systems with various end conditions and connectivity, both statically determinate and indeterminate. The issue of the appropriateness of the non-classical boundary conditions recommended in Table 1 is discussed in Section 3 where we consider the finite element solution of a cantilever beam (see comments made regarding Fig. 8). The physical implication for $\psi' = 0$ is that we account for a fully clamped condition, i.e. preventing deformation in all directions at the clamped region. This brings into consideration the actual implementation of "clamping". For example for a partially clamped end, as shown in Fig. 1(b), $\psi' \neq 0$.

To illustrate the details of the general solution, we substitute back, Eq. (11) into Eq. (12a–b), to obtain the two differential equations for the $w(x)$ and $\psi(x)$ functions that describe the solution. The differential equations are:

$$EI\left(1 + \frac{A}{I}g^2 - g^2\frac{\mathrm{d}^2}{\mathrm{d}x^2}\right)\frac{\mathrm{d}^2\psi}{\mathrm{d}x^2} = kAG\left(1 - g^2\frac{\mathrm{d}^2}{\mathrm{d}x^2}\right)\left(\frac{\mathrm{d}w}{\mathrm{d}x} + \psi\right) \tag{15a}$$

$$kAG\left(1 - g^2\frac{\mathrm{d}^2}{\mathrm{d}x^2}\right)\left(\frac{\mathrm{d}^2w}{\mathrm{d}x^2} + \frac{\mathrm{d}\psi}{\mathrm{d}x}\right) = -q \tag{15b}$$

In order to solve the two fourth order differential equations, it is convenient to set:

$$\Omega(x) = \frac{\mathrm{d}w}{\mathrm{d}x} + \psi \tag{16}$$

Eqs. (15a–b) become:

$$\left(1 - \ell^2\frac{\mathrm{d}^2}{\mathrm{d}x^2}\right)\frac{\mathrm{d}^2\psi}{\mathrm{d}x^2} = \frac{kAG}{EI}\left(\frac{\ell}{g}\right)^2\left(1 - g^2\frac{\mathrm{d}^2}{\mathrm{d}x^2}\right)\Omega \tag{17a}$$

$$\left(1 - g^2\frac{\mathrm{d}^2}{\mathrm{d}x^2}\right)\frac{\mathrm{d}\Omega}{\mathrm{d}x} = -\frac{q}{kAG} \tag{17b}$$

where ℓ is a length, which can be seen as the shear gradient internal length and is equal to:

Table 1
Beam boundary conditions (BC) and continuity requirements for the gradient Timoshenko beam.

End condition	Boundary conditions		Continuity requirements
	Classical	Non-classical	
End hinge	$w = 0, M = 0$	$Y = 0, m = 0$	–
Clamped end	$w = 0, \psi = 0$	$w' = 0, \psi' = 0$	–
Free end	$Q = 0, M = 0$	$Y = 0, m = 0$	–
Internal hinge	$M = 0$	$m = 0$	$w^+ = w^-, w'+ = w'-, w''+ = w''-, \psi^+ = \psi^-,$
Internal roller	$w = 0$	–	$\psi^+ = \psi^-, \psi'+ = \psi'-, \psi''+ = \psi''-, w'+ = w'-, w''+ = w''-, w'''+ = w'''-$

Note: In the case of concentrated moments or forces, the above BC's should be modified accordingly. This also applies to the case of intermediate supports such as springs.

$$\ell = g\sqrt{\frac{1}{1+(A/I)g^2}} \tag{18}$$

Note that when $g = 0$, $\ell = 0$ but $\ell/g = 1$. In general, ℓ/g increases with g, so $0 < \ell/g \leq 1$.

For q constant, Eq. (17b) has a general solution of the form:

$$\Omega(x) = -\frac{q}{kAG}x + c_1 e^{x/g} - c_2 e^{-x/g} + c_3 \tag{19}$$

Substituting Eq. (19) into Eq. (17a), we obtain the general solution for the ψ:

$$\psi(x) = -\frac{q}{6EI}\left(\frac{\ell}{g}\right)^2 x^3 + \frac{kAG}{2EI}\left(\frac{\ell}{g}\right)^2 c_3 x^2 + d_1\ell^2 e^{x/\ell} + d_2\ell^2 e^{-x/\ell} + d_3 + d_4 x \tag{20}$$

Substituting Eq. (20) back to Eq. (16), we obtain the general solution for the w:

$$w(x) = \left\{(c_3 - d_3)x - \frac{d_4}{2}x^2 + c_4 + d_2\ell^3 e^{-x/\ell} - d_1\ell^3 e^{x/\ell} + c_1 g^2 e^{x/g} + c_2 g^2 e^{-x/g} + \frac{q}{24EI}\left(\frac{\ell}{g}\right)^2 x^4 - \frac{q}{2kAG}x^2 - \frac{c_3 kAG}{6EI}\left(\frac{\ell}{g}\right)^2 x^3\right\} \tag{21}$$

Eqs. (20) and (21) contain a total of eight constants, c_i and d_i ($i = 1\ldots4$). These constants can be obtained from the four boundary conditions, which allow for eight independent boundary conditions (Eqs. (14a–d)).

It is interesting to examine the physical implication of the shear gradient length ℓ, since it is a function of the cross section shape and the internal length g. For a rectangular and a circular cross section respectively, the shear gradient length is:

$$\frac{\ell_{\text{rect}}}{g} = \sqrt{\frac{1}{1+12\left(\frac{g}{h}\right)^2}}, \quad \frac{\ell_{\text{circ}}}{g} = \sqrt{\frac{1}{1+16\left(\frac{g}{D}\right)^2}} \tag{22}$$

where D is the diameter of the circular cross section and h is the height of the rectangular cross section.

In Fig. 2, the normalized internal length parameter, ℓ/g, is plotted against the ratio g/h and g/D for the two cases of rectangular and circular cross sections respectively. We can observe that the shape of cross section has a minor effect on the normalized internal length.

In Fig. 3, the ratio $\ell_{\text{circ}}/\ell_{\text{rect}}$ (circular vs rectangular) is plotted against the ratio h/D for different values of the internal length g. As noted before, as g becomes negligible, the ratio $\ell_{\text{circ}}/\ell_{\text{rect}}$ approaches asymptotically the value of one. Therefore, as g becomes very small the influence of the shear gradient length is not greatly affected by the shape of the cross section. Furthermore, there is an interception point $h = 0.86D$, the same for all values of g, where $\ell_{\text{circ}} = \ell_{\text{rect}}$. It is noted that when $\ell_{\text{circ}} > \ell_{\text{rect}}$ the circular cross section is stiffer than the rectangular cross section and visa versa.

3. Examples

3.1. Isostatic beam: cantilever with a point load

We consider a cantilever beam of length L, loaded by a point load at its free end, as shown in Fig. 4. The beam has a rectangular cross section with b being the width and h the height of the cross section. In this case (Kaneko, 1975), $k = (5\nu + 5)/(6\nu + 6)$.

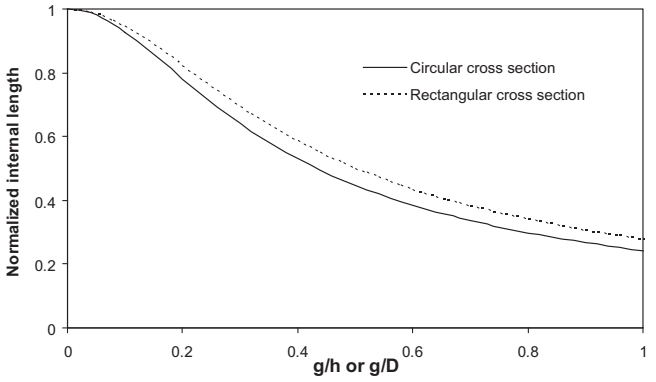

Fig. 2. Influence of the g/h or g/D, on the ratio ℓ/g for the two cases of rectangular and circular cross sections respectively.

The classic boundary conditions are:

$$w(0) = 0,\ \psi(0) = 0,\ Q(L) = P,\ M(L) = 0 \tag{23}$$

The non-classical boundary conditions are assumed to be:

$$\left.\frac{dw}{dx}\right|_{x=0} = 0,\ \left.\frac{d\psi}{dx}\right|_{x=0} = 0,\ m(L) = 0,\ Y(L) = 0 \tag{24}$$

The first two non-classical conditions imply that we want the beam to obtain maximum bending and shear stiffness, without enforcing m and Y at the fixed end. The last two conditions imply that there are no double bending moments and double shear forces at the free end.

The above conditions define a set of eight linear algebraic equations that can be solved for the eight unknown coefficients of

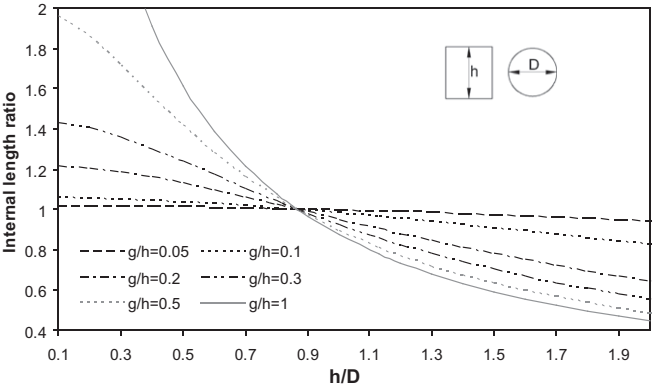

Fig. 3. Influence of the cross section shape on the gradient length g (internal length ratio of circular vs rectangular, $\ell_{\text{circ}}/\ell_{\text{rect}}$).

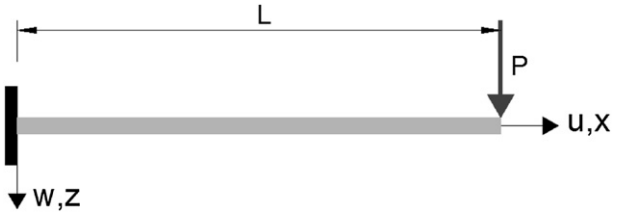

Fig. 4. Clamped beam of length L, loaded by a point load, P at its free end.

Eqs. (20) and (21). The coefficients for the case of clamped beam loaded by a point load at its free end are:

$$c_1 = -\frac{P}{kAGg\left(1+e^{2L/g}\right)},\quad c_2 = \frac{P}{kAGg}\left(\frac{e^{2L/g}}{1+e^{2L/g}}\right),$$
$$c_3 = \frac{P}{kAG},\quad c_4 = \frac{P\left(kAL\ell^4\left(1+e^{2L/g}\right)-2(1+\nu)g^3I\left(e^{2L/g}-1\right)\right)}{kAg^2EI\left(1+e^{2L/g}\right)},$$
$$d_1 = -\frac{P\ell\left(\ell e^{L/\ell}-L\right)}{EIg^2\left(1+e^{2L/\ell}\right)},\quad d_2 = -\frac{P\ell e^{L/\ell}\left(Le^{L/\ell}+\ell\right)}{EIg^2\left(1+e^{2L/\ell}\right)},$$
$$d_3 = \frac{P\ell^3\left(Le^{2L/\ell}+2\ell e^{L/\ell}-L\right)}{EIg^2\left(1+e^{2L/\ell}\right)},\quad d_4 = -\frac{PL\ell^2}{EIg^2} \tag{25}$$

The deflection at the free end of the gradient Timoshenko beam is:

$$w_{gr}(x=L) = \frac{PL^3}{3EI}\left(\frac{\ell}{g}\right)^2\left(1+3\left(\frac{\ell}{L}\right)\frac{1-e^{2L/\ell}}{1+e^{2L/\ell}} + 3\left(\frac{\ell}{L}\right)^2\frac{1+e^{2L/\ell}-4e^{L/\ell}}{1+e^{2L/\ell}} + 3\left(\frac{\ell}{L}\right)^3\frac{e^{2L/\ell}-1}{e^{2L/\ell}+1}\right) + \frac{PL}{kAG}\left(1+\left(\frac{g}{L}\right)\frac{1-e^{2L/g}}{1+e^{2L/g}}\right) = w_{gr}^b + w_{gr}^s \tag{26}$$

where w_{gr}^b is the bending part and w_{gr}^s the shear part of the deflection.

Note that Eq. (26) predicts the classical Timoshenko beam elasticity result (including the influence of shear) in the limit $g\to 0$ ($\ell/g\to 1$):

$$w_{cl} = w(x=L,\ g=0) = \frac{PL^3}{3EI}+\frac{PL}{kAG} = w_{cl}^b + w_{cl}^s \tag{27}$$

where w_{cl}^b is the bending part and w_{cl}^s the shear part of the deflection.

Note that as $G\to\infty$, $w_{cl} = w_{cl}^b$ and $w_{gr} = w_{gr}^b$, which is similar to the Bernoulli–Euler result.

The deflection at the free end of the beam predicted by the gradient Bernoulli–Euler solution (see Eq. (9) in Giannakopoulos and Stamoulis, 2006) is:

$$w_{gr\_BE}(x=L) = \frac{PL^3}{3EI}\left(1-3\left(\frac{g}{L}\right)^2\left(\cosh\left(\frac{L}{g}\right)+\frac{1}{\cosh(L/g)} + \left(\frac{L}{g}\right)\tanh\left(\frac{L}{g}\right)-1\right) + 3\left(\frac{g}{L}\right)^3\left(\tanh\left(\frac{L}{g}\right)+\left(\frac{L}{g}\right)\sinh\left(\frac{L}{g}\right)\times\tanh\left(\frac{L}{g}\right)\right)\right) = w_{gr\_BE}^b \tag{28}$$

In Fig. 5, we plot the normalized bending deflection w_{gr}^b/w_{cl}^b against the normalized parameter g/L for both the Timoshenko and Bernoulli–Euler gradient solutions assuming that $g=\ell$. This is true when $g/h << 0.3$ (see Eq. (18)). The two solutions then become identical and yield the same prediction for the deflections

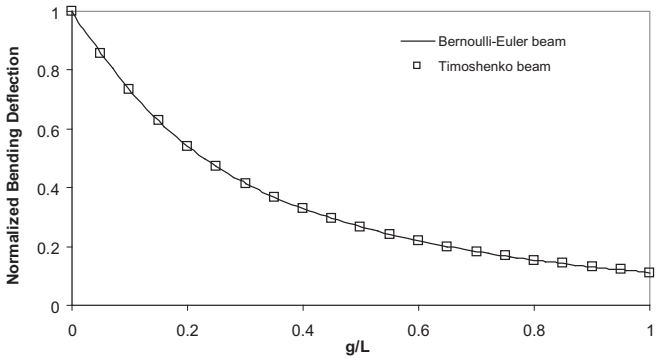

Fig. 5. Influence of g/L on the normalized bending deflection w_{gr}^b/w_{cl}^b at the free end for the gradient Timoshenko and Bernoulli–Euler prediction, assuming $g=\ell$ and $\nu=0$.

of the beam. Therefore, the Timoshenko solution reduces to the Bernoulli–Euler solution when: (a) $G\to\infty$ and (b) the scaling influence on g through the length ℓ is neglected.

In Fig. 6, we plot the normalized deflection w_{gr}/w_{cl} against the normalized parameter g/h assuming $L/h=3$ and $\nu=0$. As g/h increases, i.e. as the dimensions of the cross section of geometrically similar beams reduce, the beam becomes stiffer. Unlike the gradient Bernoulli–Euler solution, which can account only for the influence of g/L on the deflections, the gradient Timoshenko solution is able to capture the additional stiffening effect of the g/h. On the contrary, the Bernoulli–Euler prediction remains the same for beams with the same length but different cross section. In Fig. 7, we plot the normalized shear deflection w_{gr}^s/w_{cl}^s against the normalized parameter g/L for the same assumptions ($L/h=3$, $\nu=0$). The shear stiffness increases as g/L increases, but the increase in the shear stiffness is less significant than that observed in the bending part of the deflections.

We use the complete expression for the deflections of the gradient Timoshenko beam in order to compare the present model against the results from the two-dimensional finite element model derived by Giannakopoulos et al. (2006). The finite element results were derived assuming $\nu=0.26$ and are shown in Fig. 8 with the triangular symbols. The present model (gradient Timoshenko beam) matches overall the finite elements results much better than the gradient Bernoulli–Euler solution, as expected. The finite element results support our choice of boundary conditions, since considering alternative non-classical boundary conditions resulted in considerable deviation from the finite element results. Indeed, the finite element results are the only alternative engineering tool in supporting the choice of the non-classical boundary conditions.

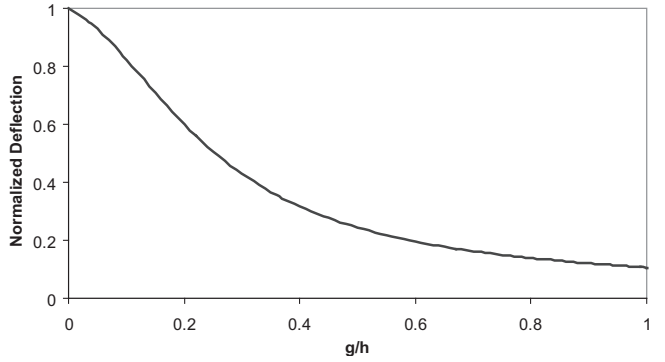

Fig. 6. Influence of g/h on the normalized deflection w_{gr}/w_{cl} at the free end for the gradient Timoshenko prediction assuming $L/h=3$ and $\nu=0$.

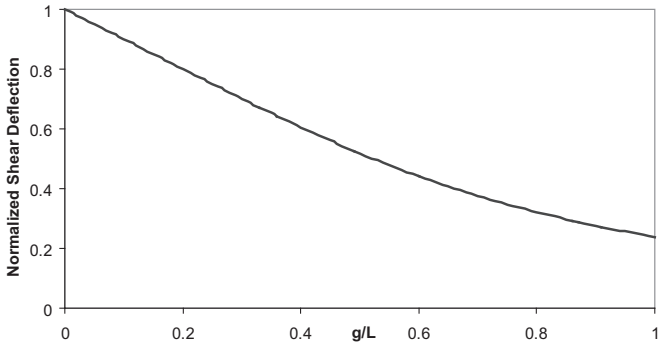

Fig. 7. Influence of g/L on the normalized shear deflection w^s_{gr}/w^s_{cl} at the free end for the gradient Timoshenko predictions assuming $L/h = 3$ and $\nu = 0$.

For quite short beams, the error is of the order of 40% and comparable to that of the Bernoulli–Euler beam. The error is rooted to the Timoshenko kinematics (see Eq. (1)) which neglects the prismatic surface boundary layers. Taking Poisson's ratio $\nu = 0$ brings the very short beam FEM results closer to the Timoshenko approximation.

Next, we consider the variation of the axial and shear strains along the length of the beam. The axial strain at the extreme fiber of the cross section, ε_{xx}, is:

$$\varepsilon_{xx}(x) = \varepsilon_0\left(\frac{\ell}{g}\right)^2\left[1-\frac{x}{L}-\frac{e^{-(x/L)(L/\ell)}\left(e^{2L/\ell}+e^{2(x/L)(L/\ell)}\right)}{1+e^{2L/\ell}} + \left(\frac{\ell}{L}\right)\frac{e^{(L/\ell)(1-(x/L))}\left(e^{2(x/L)(L/\ell)}-1\right)}{1+e^{2L/\ell}}\right] \tag{29}$$

where ε_0 is the maximum strain as predicted by classical Bernoulli–Euler beam analysis and is equal to:

$$\varepsilon_0 = \frac{PL}{Ebh^2} \tag{30}$$

The shear strain γ_{xz} is:

$$\gamma_{xz}(x) = \gamma_0\left[1-\frac{e^{(2L/g)-(x/L)(L/g)}+e^{(x/L)(L/g)}}{1+e^{2L/g}}\right] \tag{31}$$

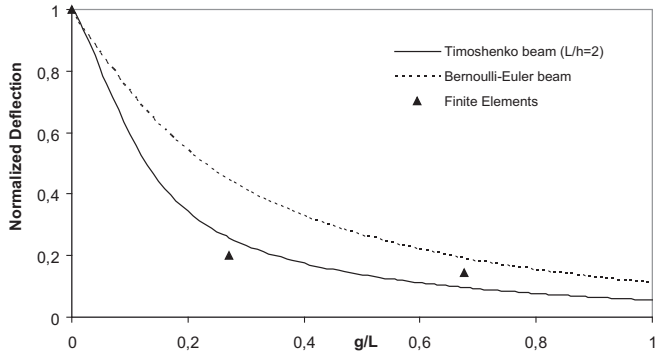

Fig. 8. Comparison between the finite element results (plain strain, $u_y = 0$), of the two-dimensional gradient model derived by Giannakopoulos et al. (2006) and the gradient Timoshenko ($L/h = 2$, $\nu = 0.26$) and gradient Bernoulli–Euler beam predictions.

where γ_0 is the shear strain as predicted by classical Timoshenko beam analysis and is equal to:

$$\gamma_0 = \frac{P}{kAG} \tag{32}$$

In Fig. 9, we plot the normalized axial strain $\varepsilon_{xx}/\varepsilon_0$ against the non-dimensional distance x/L for different values of the normalized parameter g/L for the gradient Timoshenko beam. The diamond symbols correspond to the classical Bernoulli–Euler beam prediction. The slenderness ratio assumed is $L/h = 3$ and $\nu = 0$. The solution for small values of g/L approaches asymptotically the classical Bernoulli–Euler prediction ($\varepsilon_{xx} \to \varepsilon_0$). As g/L increases the departure from the classic result becomes more significant ($\varepsilon_{xx} \to 0$). As observed in the gradient Bernoulli–Euler solution, the maximum strain does not occur at the end of the beam (see Fig. 3 in Giannakopoulos and Stamoulis, 2006). However, unlike the gradient Bernoulli–Euler solution, the gradient Timoshenko beam has approximately zero axial strain, even for large values of g/L, at the free end. The fact that the maximum strain does not occur at the clamped end of the beam is due to the imposed boundary conditions of $\psi'|_{x=0} = 0$. Actual measurements of strains on the microcantilever's clamped end, to the best of our knowledge, do not exist in the literature. Such measurements are hard to obtain due to the scale of the problem. A definite answer on whether a boundary layer exists is an issue still to be explored. However, it is interesting to note that recent fatigue tests on microcantilevers with dimensions comparable to the dimensions of the microstructure have shown that the fracture location does not occur at the root of the structure (Schwaiger and Kraft, 2003; Hocheng et al., 2004; Hocheng et al., 2008). On the other hand fatigue test on microcantilevers with completely homogeneous microstructure do fail at the root of the structure (Liu et al., 2007; Liu et al., 2008).

In Fig. 10, we plot the normalized shear strain γ_{xz}/γ_0 against the non-dimensional distance x/L for different values of the normalized parameter g/L for the gradient Timoshenko beam. The diamond symbols correspond to classical Timoshenko beam prediction. The solution for large values of g/L approaches asymptotically the classical Timoshenko beam prediction ($\gamma_{xz} \to \gamma_0$). This is the opposite of what was observed for the normalized axial strains. For very small values of g/L, the shear can be neglected ($\gamma_{xz} \to 0$), but as pointed out above, this does not mean that we recover the gradient Bernoulli–Euler solution. Furthermore, the shear becomes important as g/L increases, which can happen when the slenderness is decreased or when the microstructure length is of the same order of magnitude as the dimensions of the beam, as it should.

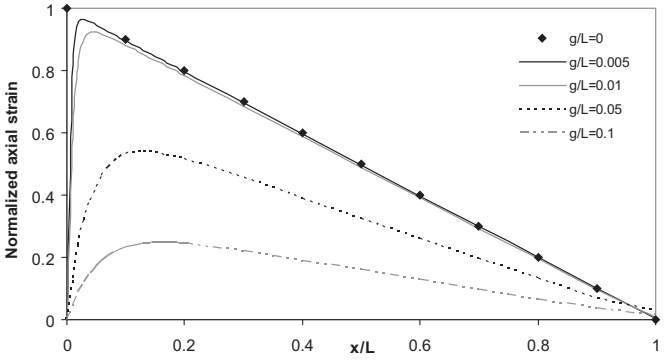

Fig. 9. Influence of the normalized parameter g/L on the normalized axial strain $\varepsilon_{xx}/\varepsilon_0$ along the length of the beam ($\nu = 0$, $L/h = 3$).

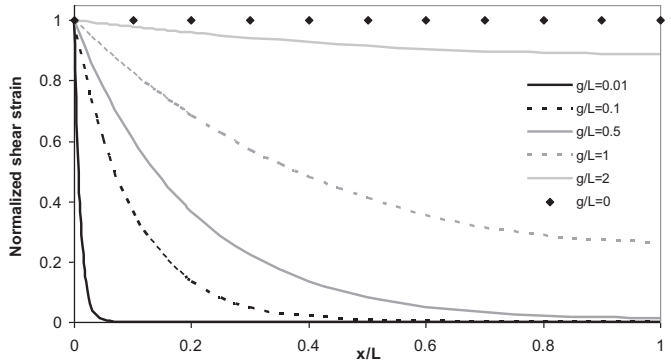

Fig. 10. Influence of the normalized parameter g/L on the normalized shear strain γ_{xz}/γ_0 along the length of the beam ($\nu = 0$, $L/h = 3$).

3.2. Hyperstatic beam: both ends fixed

Little attention has been given to the solution of statically indeterminate structural problems within the framework of gradient elasticity. In order to demonstrate how the gradient Timoshenko beam solution can be applied to such problems, we consider a cantilever beam of length L, with both ends fixed, loaded by a point load P at midspan, as shown in Fig. 11. It is noted that this beam configuration can be found in nanoscale elements (see for example Salvetat et al., 1999; Ni and Li, 2006).

Making use of the symmetry of the problem, we will model only half the beam. The boundary conditions at the fixed end are:

$$w(0) = 0,\ \psi(0) = 0,\ \left.\frac{\mathrm{d}w}{\mathrm{d}x}\right|_{x=0} = 0,\ \left.\frac{\mathrm{d}\psi}{\mathrm{d}x}\right|_{x=0} = 0 \tag{33}$$

The four additional conditions in order to define the solution at midspan are:

$$Q(L/2) = -P/2,\ \psi(L/2) = 0,\ \left.\frac{\mathrm{d}w}{\mathrm{d}x}\right|_{x=L/2} = 0,\ \left.\frac{\mathrm{d}\psi}{\mathrm{d}x}\right|_{x=L/2} = 0, \tag{34}$$

The conditions at midspan imply that the beam is in essence fixed but allowed to deflect vertically.

The coefficients for this case are:

$$\begin{aligned}
c_1 &= \frac{P}{2kAGg\left(1+\mathrm{e}^{L/2g}\right)},\ c_2 = \frac{P\mathrm{e}^{L/2g}}{2kAGg\left(1+\mathrm{e}^{L/2g}\right)},\\
c_3 &= \frac{PL}{2kAG},\ d_1 = \frac{PL\ell}{8EIg^2\left(1-\mathrm{e}^{L/2\ell}\right)},\\
c_4 &= \frac{P}{8kAg^2EI\left(1+\mathrm{e}^{L/2g}\right)}\Big(8I(1+\nu)g^3 - 8I\mathrm{e}^{L/2g}(1+\nu)g^3\\
&\qquad + kAL\ell^4\left(1+\mathrm{e}^{L/2g}\right)\Big),\\
d_2 &= \frac{PL\ell\mathrm{e}^{L/2\ell}}{8EIg^2\left(1-\mathrm{e}^{L/2\ell}\right)},\ d_3 = \frac{PL\ell^3\left(\mathrm{e}^{L/2\ell}+1\right)}{8EIg^2\left(\mathrm{e}^{L/2\ell}-1\right)},\\
d_4 &= -\frac{PL\ell^2\left(L^2+2\ell^2\right)}{8EIg^2}
\end{aligned} \tag{35}$$

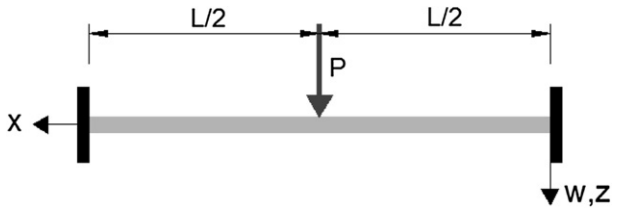

Fig. 11. Beam of length L, with both ends clamped, loaded by a point load P at midspan.

We will not repeat here the plots and details of the solution as in Section 3.1, since all comments and remarks hold true regardless of the loading and support conditions. We will simply present the prediction for the maximum deflection at midspan:

$$\begin{aligned}
w_{\mathrm{gr}}(x = L/2) = \frac{PL^3}{192EI}\left(\frac{\ell}{g}\right)^2\Bigg(1 + 12\left(\frac{\ell}{L}\right)\frac{1+\mathrm{e}^{L/2\ell}}{1-\mathrm{e}^{L/2\ell}}\\
+ 24\left(\frac{\ell}{L}\right)^2\frac{1+2\mathrm{e}^{L/2g}}{1+\mathrm{e}^{L/2g}}\Bigg)\\
+ \frac{PL}{4kAG}\left(1 + 4\left(\frac{g}{L}\right)\frac{1-\mathrm{e}^{L/2g}}{1+\mathrm{e}^{L/2g}}\right)
\end{aligned} \tag{36}$$

In the limit, $g \to 0$, the classic Timoshenko beam prediction is recovered:

$$w_{\mathrm{cl}} = w(x = L,\ g = 0) = \frac{PL^3}{192EI} + \frac{PL}{4kAG} \tag{37}$$

If, in addition $G \to \infty$, we obtain the classical Bernoulli–Euler prediction $PL^3/(192EI)$.

4. Comparison of non-local Timoshenko beam models

It is interesting to compare our solution with other gradient Timoshenko beam solutions available in the bibliography. Non-local Timoshenko beam models have been proposed by Lam et al. (2003), Ma et al. (2008), Wang et al. (2010), Asghari et al. (2011) and Lazopoulos and Lazopoulos (2011). We consider the example of an epoxy beam with the following material properties: $E = 1.44$ GPa, $\nu = 0.38$ and $g = 17.6$ μm. The beam's length, width and height respectively are: $L = 10h$, $b = 2h$ and $h = 2g$. The load is $P = 50$ μN. Note that most of the above authors have considered the similar case of a simply supported beam loaded by a point load at midspan. The maximum deflection of the cantilever beam is equal to the maximum deflection of a simply supported beam, if we set the load and length of the cantilever beam to be half of those considered for the simply supported beam (i.e. for the simply supported beam $P = 100$ μN and $L = 20h$). It is noted that only Lam et al. (2003), Asghari et al. (2011) and the present work have solved the problem in close form. The other works use Fourier series to describe the solution to the problem. Table 2, lists the normalized maximum deflection prediction for each model.

All these models assume the same Timoshenko kinematic assumptions and all can capture the size effect in stiffness. As it can be seen in Table 2, dipolar elasticity models give stiffer response than both the micropolar and couple stress models, as it should. Furthermore micropolar elasticity models give stiffer response than the couple stress models as expected.

Two other Timoshenko beam models have been reported in Lazopoulos and Lazopoulos (2011) and Wang et al. (2010) using the same dipolar strain gradient theory. In particular, Wang et al. (2010) use three material lengths (ℓ_0, ℓ_1, ℓ_2) that are taken equal in their numerical examples. Lazopoulos and Lazopoulos (2011) have correctly used the principle of minimum potential energy (apart for some typos) and have come up with four (4) boundary conditions (BC), as in the present work. However, instead of enforcing $M = m = 0$ at the hinge supports, they have used $\psi = \psi' = 0$ (compare the recommendations of Table 1 of this work and Eq. (25) in Lazopoulos and Lazopoulos, 2011). Although the variational principle allows their choice of these BC, a hinge support implies absence of bending moment and in the case of a gradient beam, absence of double bending moment as well, something which by choosing $\psi = \psi' = 0$ is not satisfied. In the case of Wang et al.

Table 2
Maximum prediction estimated of different non-local Timoshenko beam models for the specific case of an epoxy beam (the internal length is taken the same in all cases).

Non-local Timoshenko model	w_{cl}/w_{gr}
Dipolar elasticity	
Present	4.12
Lazopoulos and Lazopoulos (2011)	3.85
Wang et al. (2010)	3.00
Micropolar elasticity	
Lam et al. (2003)	2.19
Couple stress elasticity	
Ma et al. (2008)	1.58
Asghari et al. (2011)	1.59

(2010), in their minimization principle, the term associated with $\delta w'$, was attributed to the work done by the bending moment M and not to the double shear forces Y, as we have done so. Actually they do not prescribe the double shear force quantity at all in the expression of the work done by the external forces. By doing so however, the term $\delta\psi$ in the strain energy has no equivalent in the expression of the external work (see Eqs. (27) and (30) in Wang et al., 2010). We believe that since the inclusion of axial stress gradient results in double bending moment, the inclusion of shear gradients should result in double shear forces. Furthermore, double shear forces should be treated as a separate quantity than the classical bending moment, although their dimensions are the same. For this reason, although their formulation requires four (4) boundary conditions, one of them, i.e. the BC steaming from $\delta\psi$ is suppressed (see Eq. (35) in Wang et al., 2010). Regarding their choice of BC, they assumed the same BC with the couple stress model of Ma et al. (2008), but this is possible for the particular choice of the Fourier series expansion for w and ψ that was assumed in their work.

Next we consider the three works (present, Lam et al., 2003; Asghari et al., 2011) that solve the problem in close form and compare their predictions in the case of a less slender beam. We consider the same example as before only this time we set the length to be: $L = 5h$. The w_{cl}/w_{gr} ratio for the present, the Lam et al. (2003) and the Asghari et al. (2011) models becomes 4.42, 2.19 and 12.35 respectively. Assuming half the slenderness didn't affect the Lam et al. (2003) prediction since this model only accounts for the influence of the g/h ratio. If g/h is kept the same, any changes in the slenderness of the beam will not affect their prediction. Both, the present and the Asghari et al. (2011) models predict an increase of the stiffness. However the Asghari et al. (2011) model shows a surprising increase, since their model predicts that the stiffness will increase almost eight times as the g/L ratio goes from 0.05 to 0.1.

The aforementioned comparisons assumed the same value for the internal length. Clearly all theories can be forced to give the same stiffness, if the material length is taken appropriately (as we will see in the next section). How appropriate each theory is, depends on the material system. Consistency of a theory requires testing independent configurations of the same material, e.g. cantilever and clamped at both end beams, or simply shorter beams. To the best of our knowledge such tests do not exist.

5. Experimental evidence

In this section, we use experiments on microcantilevers available in the bibliography in order to explain the size effect observed. Furthermore, we compare our predictions of the microstructural length with the predictions of micropolar elasticity in order to illustrate another import issue concerning the validity of non-local models.

Micropolar elasticity (Lam et al., 2003) predicts that the stiffness of a cantilever beam ($K = \mathrm{d}P/\mathrm{d}w_{gr}$) is:

$$K = K_{cl}\left[1 + \left(\frac{\widehat{b}_h}{h}\right)^2\right] \tag{38}$$

where K_{cl} is the classical prediction and $\widehat{b}_h$ is a length parameter which is equal to:

$$\widehat{b}_h^2 = (10.6 - 15.4\nu)\lambda^2 \tag{39}$$

where λ is the micropolar elasticity length, if all the material length scale parameters are assumed to be the same.

McFarland and Colton (2005) tested polypropylene (PP, Basel/Montell ProFax 6323) microcantilever beams manufactured via injection molding with two different mold geometries and compared the measured stiffness of the beams. The geometry of the microcantilevers and their relative stiffness (K_{exp}/K_{cl}) are summarized in Table 3. The last two columns of Table 3, lists the estimates of the internal length obtained from the gradient Timoshenko beam solution and micropolar elasticity respectively.

Lam et al. (2003) tested epoxy polymeric (Bisphenol-A epichlorohydrin resin with 20 phr diethylenetriamine hardener) microcantilevers fabricated by casting. The beams have the same slenderness ratio and four different thicknesses. The geometry of the microcantilevers and their relative stiffness (K_{exp}/K_{cl}) are summarized in Table 4 (see Fig. 12 in Lam et al., 2003). The last two columns of Table 4, lists the estimates of the internal length obtained from the gradient Timoshenko beam solution and micropolar elasticity respectively. Our model predicts the internal length to be 6.73 ± 15% μm. Micropolar elasticity predicts the length to be 10.61 ± 17% μm.

Ding et al. (2001a) tested LPCVD polysilicon microcantilevers keeping the same thickness and varying the L/h ratio. They used these bending experiments to derive an estimate for the modulus of elasticity, E, using the classic elasticity predictions. However, in a separate paper (Ding et al., 2001b), the same authors, tested in tension exactly the same material and found a different value for the modulus of elasticity. We use the modulus of elasticity estimate derived by tension experiments to interpret the bending experiments and we found that the beams exhibit a stiffer response than that predicted by classic elasticity. The geometry of the microcantilevers and their relative stiffness (K_{exp}/K_{cl}) are summarized in Table 5. The last two columns of Table 5, list the estimates of the internal length obtained from the gradient Timoshenko beam solution and micropolar elasticity respectively. Our model predicts the internal length to be 0.29 ± 13% μm. Micropolar elasticity predicts the length to be 0.42 ± 14% μm.

Hong et al. (2005) tested Cu microcantilevers keeping the same width and varying the L/h ratio. They used these bending experiments to derive an estimate for the modulus of elasticity, E, using the classic elasticity predictions. Huang and Spaepen (2000) conducted uniaxial tensile experiments on Cu thin films and reported

Table 3
Geometry and results for the polypropylene microcantilevers tested by McFarland and Colton (2005).

E (GPa)	ν	L (μm)	b (μm)	h (μm)	K_{exp}/K_{cl}	g[a] (μm)	λ[b] (μm)
3.3	0.3	836	125	29.37	5.075	16.87	24.24
3.1		398	123	15.85	4.347	8.23	11.86

[a] Estimate of the material length based on strain gradient Timoshenko solution.
[b] Estimate of the material length based on micropolar elasticity solution.

Table 4
Geometry and results for the epoxy polymeric microcantilevers tested by Lam et al. (2003).

E (GPa)	ν	h (μm)	Slenderness L/h	K_{exp}/K_{cl}	g^a (μm)	λ^b (μm)
1.5	0.3	20	10	2.357	6.41	9.53
		38		1.321	5.72	8.80
		75		1.143	7.27	11.60
		115		1.071	7.51	12.53

[a] Estimate of the material length based on strain gradient Timoshenko solution.
[b] Estimate of the material length based on micropolar elasticity solution.

the value for the Young's modulus. We use the uniaxial value and compare the experimental stiffness reported with the one predicted by classical elasticity. The geometry of the microcantilevers and their relative stiffness (K_{exp}/K_{cl}) are summarized in Table 6. The last two columns of Table 6, list the estimates of the internal length obtained from the gradient Timoshenko beam solution and micropolar elasticity respectively.

Obviously, all non-local theories can predict a microstructural length and the magnitude of this length will vary depending on the theory used. Nevertheless, consistency of a theory requires this prediction to be the same for different geometries, if the same material is under consideration. Both non-local theories predict an average value with approximately the same error. Furthermore both theories are able to explain the size effect measured in the experiments, and quantify the departure form the classical elasticity predictions. The main difference is in the magnitude of the internal length predicted by the two theories. The micropolar length is approximately 50% greater than the dipolar length ($\lambda \cong 1.5 \times g$).

As mentioned in the introduction, the microstructural length parameter is associated with the microstructure of the material in an average sense. In other words, the exact physical correlation between the internal length and the dominant feature of a material's microstructure is a topic still open. The simplest correlation would be for the internal length to be equal to the size of the dominant feature of the microstructure. From the experimental results included in this section, only Ding et al. (2001a) provide information about the microstructure of the material used in the bending experiments (grain size of polysilicon was in the order of 0.2 μm). Our model predicts the internal length to be $0.29 \pm 13\%$ μm, whereas Micropolar elasticity predicts the length to be $0.42 \pm 14\%$ μm. It seems that our model successfully predicts the size effect dependence on the microstructure's scale in this particular case. Concerning the other three experimental works, information concerning the microstructure is not provided by the authors. The prediction of both theories falls within the typical range of values for the microstructure scale for these materials. In the absence of the explicit information for the material used in the experiment, no conclusion on which theory is more accurate can be made.

Nevertheless, the correlation between the dominant feature of the microstructure and the internal length may be more complex. For example, size effect has also observed on ZnO nanobelts with the structures being stiffer as the diameter of the cross section decreased from 40 nm to 10 nm (Ni and Li, 2006). Although the ZnO nanobelts are single crystalline (wurtzite-structured) and can be seen as homogeneous materials, their source of size effect is somehow geometric. Essentially, as the scale decreases, the surface-to-volume ratio increases considerably and this results in more atoms being at the surface than in the bulk. When deformation occurs, the surface reconstruction affects the mechanical properties of the nanowire. This was sufficiently explained by Kulkarni et al. (2005) by molecular dynamics simulations, but can be equivalently explained in the context of gradient elasticity, if an internal length is assumed. Obviously this line of thinking is rather speculative at this point, but as structures are pushed to the limit, surface effects could provide explanation on why even materials that are homogeneous in the atomic level will exhibit size effect.

Finally, the difference between the predicted internal length values leads to another important observation regarding the limitation of both theories. Although the formulas allow for any value of the internal length, it is tacitly presupposed that the microstructural length is of the same order or less than the dimensions of the cross section, otherwise the assumption of a continuum is compromised. In other words, the prediction must satisfy that g/h or λ/h is less than or equal to one. Son et al. (2003) performed cantilever bending tests on thin films of aluminum and gold with grain size to thickness ratio close to one and in some cases greater than one. In this extreme limit, it is questionable whether isotropic gradient theories are still applicable. Micropolar elasticity reaches this threshold for smaller stiffness rations than the present strain gradient Timoshenko model.

Table 5
Geometry and results for the LPCVD polysilicon microcantilevers tested by Ding et al. (2001a).

E^c (GPa)	ν	L (μm)	b (μm)	h (μm)	K_{exp}/K_{cl}	g^a (μm)	λ^b (μm)
164	0.23	16	50	2.4	1.215	0.278	0.425
		34	40		1.209	0.295	0.413
		31	40		1.154	0.248	0.354
		18	10		1.276	0.324	0.475

[a] Estimate of the material length based on strain gradient Timoshenko solution.
[b] Estimate of the material length based on micropolar elasticity solution.
[c] The Young's modulus, E, is derived from tension experiments (see Ding et al., 2001b).

Table 6
Geometry and results for the copper (Cu) microcantilevers tested by Hong et al. (2005).

E^c (GPa)	ν	L (μm)	b (μm)	h (μm)	K_{exp}/K_{cl}	g^a (μm)	λ^b (μm)
102	0.31	129	50	10.5	1.021	0.361	0.630
		104	50	2.8	1.177	0.351	0.497

[a] Estimate of the material length based on strain gradient Timoshenko solution.
[b] Estimate of the material length based on micropolar elasticity solution.
[c] The Young's modulus, E, is derived from tension experiments (see Huang and Spaepen, 2000).

6. Conclusions

The governing equations and boundary conditions were derived for a strain gradient Timoshenko beam using a simplified (dipolar) strain gradient theory of only one additional material length. The problem was solved in closed-form and we have provided a methodology for solving more complex beam problems, i.e. hyperstatic beam configurations. This model reduces to the gradient Bernoulli–Euler solution and to the classical Timoshenko solution, when the necessary simplifications and limits are considered and also matches very well the two-dimensional finite element model. Furthermore, the present model was used to interconnect the size effect observed in experiments of microcantilevers, obtaining good results regarding the material length. Finally, we compare our model with the micropolar elasticity model and we found that both can capture the size effect in a consistent manner, but our model predicts approximately 50% smaller values for the internal length than micropolar elasticity.

Acknowledgments

The current work is part of the "Hrakleitos II" project of the Greek Ministry of National Education for basic research on size effect phenomena.

References

Asghari, M., Kahrobaiyan, M.H., Rahaeifard, M., Ahmadian, M.T., 2011. Investigation of the size effects in Timoshenko beams based on the couple stress theory. Arch. App. Mech. 81, 863–874.

Cosserat, E., Cosserat, F., 1909. Theorie des Corps Deformables. Hermann et Fils, Paris.

Ding, J.N., Meng, Y.G., Wen, S.Z., 2001a. Specimen size effect on mechanical properties of polysilicon microcantilever beams measured by deflection using a nanoindenter. Mater. Sci. Eng.:B 83, 42–47.

Ding, J.N., Meng, Y.G., Wen, S.Z., 2001b. Size effect on the mechanical properties and reliability analysis of microfabricated polysilicon thin films. Reliability Physics Symposium. Proc. Int. Rel. Phys. Symp. pp. 106–111.

Eringen, A.C., 1966. Linear theory in micropolar elasticity. J. Math. Mech. 15, 909–923.

Giannakopoulos, A.E., Stamoulis, K., 2006. Structural analysis of gradient elastic components. Int. J. Solids Struct. 44, 3440–3451.

Giannakopoulos, A.E., Amanatidou, E., Aravas, N., 2006. A reciprocity theorem in linear gradient elasticity and the corresponding Saint-Venant principle. Int. J. Solids Struct. 43, 3875–3894.

Hocheng, H., Kao, K.S., Fang, W., 2004. Fatigue life of a microcantilever beam in bending. J. Vac. Sci. Technol. B 22 (6), 3143–3146.

Hocheng, H., Hung, J.-N., Guu, Y.-H., 2008. Various fatigue testing of polycrystalline silicon microcantilever beam in bending. Jap. J. Appl. Phys. 47 (6), 5256–5261.

Hong, S.H., Kim, K.S., Kim, Y.-M., Hahn, J.-H., Lee, C.-S., Park, J.-H., 2005. Characterization of elastic moduli of Cu thin films using nanoindentation technique. Comp. Sci. Tech. 65, 1401–1408.

Huang, H., Spaepen, F., 2000. Tensile testing of free standing Cu, Ag and Al thin films and Ag/Cu multilayers. Acta Mater. 48, 3261–3269.

Jager, I., Fratzl, P., 2000. Mineralized collagen fibrils: a mechanical model with staggered arrangement of mineral particles. Biophys. J. 79, 1739–1746.

Kaneko, T., 1975. On Timoshenko's correction for shear in vibrating beams. J. Phys. D: Appl. Phys. 8, 1927–1936.

Koiter, W.T., 1964. Couple stresses in the theory of elasticity. I & II. P. K. Ned. Akad. Wet. Ser. B 67, 17–44.

Kulkarni, A.J., Zhou, M., Ke, F.J., 2005. Orientation and size dependence of the elastic properties of zinc oxide nanobelts. Nanotechnology 16, 2749–2756.

Lam, D.C.C., Yang, F., Chong, A.C.M., Tong, P., 2003. Experiments and theory in strain gradient elasticity. J. Mech. Phys. Solids 51, 1477–1508.

Lazopoulos, K.A., Lazopoulos, A.K., 2011. On the strain gradient Timoshenko beam model. J. Appl. Math. Mech. 91 (11), 875–882.

Liu, H.-K., Lee, B.J., Liu, P.-P., 2007. Low cycle fatigue of single crystal silicon thin films. Sens. Act. A 140, 257–265.

Liu, H.-K., Pan, C.H., Liu, P.-P., 2008. Dimension effect on mechanical behavior of silicon micro-cantilever beams. Measurement 41, 885–895.

Ma, H.M., Gao, X.-L., Reddy, J.N., 2008. A microstructure-dependent Timoshenko beam model based on a modified couple stress theory. J. Mech. Phys. Solids 56 (12), 3379–3391.

McFarland, A.W., Colton, J.S., 2005. Role of materials microstructure in plate stiffness with relevance to microcantilever sensors. J. Micromech. Microeng. 15, 1060–1067.

Mindlin, R.D., 1964. Micro-structure in linear elasticity. Arch. Rat. Mech. Anal. 16, 51–78.

Morgan, R.J., O'Neal, J.E., 1977. The microscopic failure processes and their relation to the structure of amine-cured bisphenol-A-diglycidyl ether epoxies. J. Mater. Sci. 12, 1966–1980.

Namarazu, T., Isono, Y., Tanaka, T., 2000. Evaluation of size effect on mechanical properties of single crystal silicon by nanoscale bending test using AFM. J. Microelectromech. Syst. 9 (4), 450–459.

Ni, H., Li, X., 2006. Young's modulus of ZnO nanobelts measured using atomic force microscopy and nanoindentation techniques. Nanotechnology 17, 3591–3597.

Papargyri-Beskou, S., Tsepoura, K.G., Polyzos, D., Beskos, D.E., 2003. Bending and stability analysis of gradient elastic beams. Int. J. Solids Struct. 40, 385–400. Erratum: 42, 4911–4912.

Papargyri-Beskou, S., Polyzos, D., Beskos, B.E., 2009. Wave dispersion in gradient elastic solids and structures: a unified treatment. Int. J. Solids Struct. 46, 3751–3759.

Perez-Prado, M.T., Vlassak, J.J., 2002. Microstructural evolution in electroplated Cu thin films. Scr. Mater. 47, 817–823.

Poncharal, P., Wang, Z.L., Ugarte, D., de Heer, A.W., 1999. Electrostatic deflections and electromechanical resonances of carbon nanotubes. Science 283, 1513–1516.

Ramezani, S., Naghdabadi, R., Sohrabpour, S., 2009. Analysis of micropolar elastic beams. Eur. J. Mech. A/Solids 28, 202–208.

Reddy, J.N., 2007. Non-local theories for bending, buckling and vibration of beams. Int. J. Eng. Sci. 45, 288–307.

Ru, C.Q., Aifantis, E.C., 1993. A simple approach to solve boundary value problems in gradient elasticity. Acta Mech. 101, 59–68.

Salvetat, J.P., Briggs, A.D., Bonard, J.M., Basca, R.B., Kulik, A.J., Stockli, T., Burnham, N.A., Forro, L., 1999. Elastic and shear moduli of single-walled carbon nanotube ropes. Phys. Rev. Lett. 82 (5), 944–947.

Schwaiger, R., Kraft, O., 2003. Size effect in the fatigue behavior of thin Ag films. Acta Mater. 51, 195–206.

Senturia, S.D., 2001. Microsystem Design. Kluwer Academic Publishers, Boston.

Son, D., Jeong, J.H., Kwon, D., 2003. Film-thickness considerations in microcantilever-beam test in measuring mechanical properties of metal thin film. Thin Solid Films 437, 182–187.

Timoshenko, S.P., Goodier, J.N., 1970. Theory of Elasticity, third ed. McGraw–Hill, New York.

Vanlandingham, M.R., Eduljee, R.F., Gillespie Jr., , 1999. Relationships between stoichiometry, microstructure, and properties for amine-cured epoxies. J. Appl. Polym. Sci. 71 (5), 699–712.

Vardoulakis, I., Sulem, J., 1995. Bifurcation Analysis in Geomechanics. Blackie/Chapman & Hall, London.

Vianna, J.C., Cunha, A.M., Billon, N., 2002. The thermomechanical environment and the microstructure of an injection moulded polypropylene copolymer. Polymer 43, 4185–4196.

Wang, B., Zhao, J., Zhou, S., 2010. A micro scale Timoshenko beam model based on strain gradient elasticity theory. Eur. J. Mech. A/Solids 29, 591–599.

Yang, L., Van der Werf, K.O., Fitie, C.F.C., Bennink, M.L., Dijkstra, P.J., Feijen, J., 2008. Mechanical properties of native and cross-linked type I collagen fibrils. Biophys. J. 94, 2204–2211.